RSC Advances

PAPER

Check for updates

Corrosion protection properties of tetraphenylethylene-based inhibitors toward carbon steel in acidic medium†

Yumeng Chen,‡ Yiming An,‡ Jing Ma, Zhihua Zhang, Fulin Qiao, Xue Lei, Fei Sun, [ID] * Chunlu Wang,* Song Gao, Yue Zhao, Jinhua Wang, Xiaoping Fu, Hui Wang and Zhengqi Yu

Four novel corrosion inhibitors (**1**, **2**, **3** and **4**) integrating different tetraphenylethylene (TPE) cations and thiocyanate (SCN⁻) anions were developed. Weight-loss and electrochemical measurements were employed to assess their protective properties toward carbon steel in 0.5 M H_2SO_4, revealing them as effective corrosion inhibitors in the order of **3** > **4** > **2** > **1**, with the inhibition efficiencies of **2**, **3** and **4** all exceeding 97%. The inhibitory effect could be attributed to hard and soft acids and bases theory and the synergistic effect of the charged ingredients. The efficiency trend of the corrosion inhibition, as well as inhibition mechanism, was verified by multi-scaled theoretical simulations combined with grand canonical Monte Carlo and molecular dynamic methods.

1. Introduction

Metal corrosion is a ubiquitous and long-standing phenomenon in daily life and industrial operation. It can deteriorate the functionality, shorten the life span and raise the maintenance costs of a metal or alloy. Furthermore, corrosion poses a great threat to engineering quality, public safety, and huge economic loss.[1,2] Due to the favorable properties such as good mechanical flexibility, high thermal and electrical conductivity, and cost-effective performance, carbon steel is intensively utilized in the petrochemical industry, pipeline transportation, power plants, marine, military, and so on. Unfortunately, carbon steel is susceptible to corrosion under various conditions including acidic solution, microbiological environment, oxygen-rich medium, and high conductivity medium.[3-8] Corrosion cannot be utterly prohibited, but corrosion rate can be alleviated *via* adoption of effective protection methods. It's estimated that 20–30% of corrosion losses could be avoided if adequate protective measures are adopted.[9,10] Currently, the usage of corrosion inhibitors is one of the most practical and cost-effective methods in industry. Corrosion inhibitors can be adsorbed onto metal surface, forming a protective layer that isolates metal surface from corrosive species. Hence, the search and development of novel inhibitors with high inhibitory capacity is always in great demand.[10-17] In general, conventional corrosion inhibitors are organic compounds containing hetero atoms (O, N, S, or P) and aromatic rings or long alkyl chains, for example, imidazole, pyrimidine, triazole, guanidine, acridine, Schiff-bases, *etc.*[9,18-22] Particularly, inhibitor molecule with a relatively larger hydrophobic and conjugated skeleton could resist corrosion more effectively, in terms of surface coverage and electron donor–acceptor interaction with metal atoms.[23-26]

Tetraphenylethylene (TPE) bearing a central olefin and four peripheral phenyl rings, is a well-known and widely studied AIEgen – a luminogen possessing the unique character of aggregation-induced emission (AIE).[27] Since originally reported by Tang's group in 2001,[28] AIEens have been elaborately investigated and utilized in numerous ranges, for instance, chemical sensing, biomedical fields, optoelectronic systems, and stimuli responses.[27,29-34] AIEgens are almost non-emissive in monomer state, *e.g.* in dilute solution, but become highly emissive in aggregation state, *e.g.* in solid or gel state. The working mechanism is attributed to the restriction of intramolecular motions (RIM).[27,35] TPE has been studied with metal ions or complexes, including gelation, sensors, nanoparticles, metal–organic frameworks.[36-40] Nevertheless, TPE and other AIEgens have been scarcely investigated on the surface of metal or alloy,[41] not to mention being developed as corrosion inhibitors.

In this study, four novel corrosion inhibitors (**1**, **2**, **3** and **4**) integrating different TPE cations and thiocyanate anions (SCN⁻) were developed. The TPE unit was taken advantage of its large hydrophobic and conjugated skeleton, along with its AIE effect. The counter anion SCN⁻, deemed as a soft Lewis base, was used for its intense interaction with steel surface, which acted as a soft acid in light of hard and soft acids and bases (HSAB) theory. These four inhibitors exerted effective protective

Sinopec Research Institute of Petroleum Processing Co., Ltd., Beijing 100083, P. R. China. E-mail: sunfei.ripp@sinopec.com; wcl.ripp@sinopec.com

† Electronic supplementary information (ESI) available. See DOI: https://doi.org/10.1039/d2ra08062a

‡ Yumeng Chen and Yiming An contributed equally to this paper.

properties toward carbon steel in highly acidic medium. Notably, the inhibition efficiencies of **2**, **3** and **4** all exceeded 97%.

2. Materials and methods

2.1 Materials and instruments

All reagent chemicals including tetraphenylethylene, RANEY® nickel, hydrazine hydrate, sodium thiocyanate, HNO_3, H_2SO_4 were commercially purchased from Alfa Aesar, Sinopharm Chemical Reagent Co., Ltd., and Beijing Chemical Works in analytical grade or chemically pure, and used as received. The test solution, 0.5 M H_2SO_4 (treated as blank), was diluted from concentrated H_2SO_4.

Carbon steel coupons with the dimensions of 40 mm × 13 mm × 2 mm were purchased from Gaoyou City Xinyou Instrument Plant. The element content of carbon steel coupon is shown in Table 1.

Instrumental information and methodology of ^1H NMR, ^{13}C NMR, high-resolution mass spectra (HRMS, ESI), UV-Vis absorption spectra, fluorescence (FL) spectra, X-ray photoelectron spectroscopy (XPS) spectra, scanning electron microscope (SEM) images are provided in ESI.†

2.2 Chemical structures of TPE-based inhibitors

The structures and synthetic routes of four TPE-based corrosion inhibitors (**1**, **2**, **3** and **4**) are presented in Fig. 1. The synthesis of the inhibitors started from tetraphenylethylene (TPE), and the detailed procedures are provided in ESI.†

2.3 Weight-loss measurement

Weight-loss measurement is a traditional and intuitive method to inspect the corrosion rate of metal or alloy, which is the basis of other measurements. In this work, weight-loss measurements were carried out with carbon steel coupons soaked in 0.5 M H_2SO_4 solutions without or with various concentrations of the TPE-based inhibitors at 60 °C, constantly agitated by a magnetic stir bar. The detailed procedures are presented in

ESI.† The corrosion rate (v) and inhibition efficiency (η) are calculated through subsequent equations:

$$v = (W_0 - W_1)/(\rho St) \tag{1}$$

$$\eta = (v_0 - v_1)/v_0 \times 100\% \tag{2}$$

where W_0 and W_1 represent the weights of coupon before and after soak experiment; ρ denotes the density of carbon steel; S is the superficial area of coupon; t is the time of soak experiment; v_0 represents the corrosion rate in the blank solution without any inhibitor; v_1 is the corrosion rate in an inhibitor containing solution.

2.4 Electrochemical measurements

Electrochemical measurements were carried out in a traditional three-electrode electrochemical system using CHI760 electrochemical workstation. Carbon steel was used as working electrode with 1 cm^2 exposed area. Platinum electrode and saturated calomel electrode (SCE) were employed as counter electrode and reference electrode, respectively. Aqueous 0.5 M H_2SO_4 solution was used as electrolyte with continuous stir using magnetic stirring bar. The electrodes were immersed in the electrolyte for 1 h before test. Electrochemical impedance spectroscopy (EIS) measurements were performed with potential amplitude within ±5 mV relative to OCP and test frequency ranging from 0.01 Hz to 100 kHz. And the potentiodynamic polarization (PDP) curves were measured at a constant sweep rate of 0.5 mV s^{-1}.

2.5 Theoretical calculations

To model the corrosion process, a periodic metal surface of Fe was first built. Since Fe (110) surface is relatively compact and stable plane over other Fe surfaces as well as its highest proportion in Fe lattice,[25,42] the primitive cell of iron lattice was cleaved alone (110) plane after optimization and then expanded to a 6 layered supercell of (12 × 9) periodic box with a 25 Å vacuum slab. The dimension of the final surface model was 33.10 Å × 35.10 Å × 35.75 Å with sufficient surface area to avoid mutual interference among periodic structures. All Fe atoms' cartesian positions were fixed for all simulations (Fig. 2).

Both Grand Canonical Monte Carlo (GCMC) and Molecular Dynamic (MD) simulations were performed by modules in BIOVIA Material Studio 2017 software package. The adsorption

Table 1 Element content of carbon steel coupon

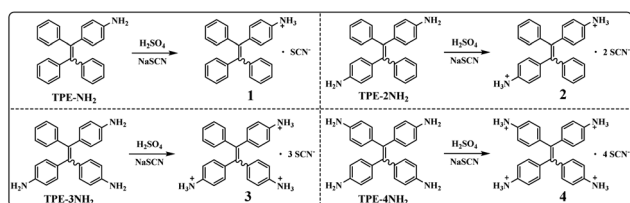| Element	C	Fe	Si	Mn	P	S	V
wt%	0.34	Balance	0.20	1.45	0.01	0.009	0.11

Fig. 1 Scheme for the synthesis of TPE-based corrosion inhibitors (**1**, **2**, **3** and **4**).
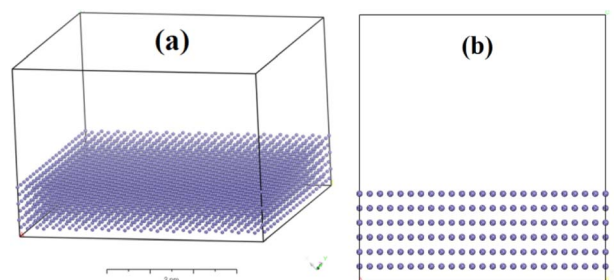

Fig. 2 Illustration of carbon steel model. Blue dot: Fe atom.

module was used for GCMC simulations and Forcite module was used for MD simulations. A UFF forcefield was employed for both modules in order to cover all elements involved in the modelling system, which has proved its reliability and wide application scope.[43,44] The charge setting of modelling systems for both modules were set with ESP charge obtained from DFT optimizations. The probability of conformer, rotate, translate, regrow were set to 0.32, 0.32, 0.32, 0.03, respectively for GCMC simulations, with 1000 cycles and 500 steps per cycle. For MD simulations the initial adsorption configurations were based on GCMC results, the temperature was set to 298 K in accordance with actual application condition, and the total dynamic simulation time was set to 5000 ps with time step of 1.0 fs. A pearl script was used to process obtained trajectories for energy of interaction (E_{int}) calculation.

3. Results and discussions

3.1 Weight-loss measurement

Weight-loss measurements for carbon steel have been conducted in 0.5 M H_2SO_4 with varying concentrations of the TPE-based inhibitors, and the results are shown in Fig. 3. The photographs of coupons after measurements are presented in Fig. 4. It is found carbon steel corroded heavily in 0.5 M H_2SO_4 in the absence of any inhibitor (blank sample), with the corrosion rate exceeding 150 mm a^{-1}. However, the four inhibitors (1, 2, 3 and 4) exerted effective protection for carbon steel, with apparent mitigation of corrosion rate and elevation of inhibition efficiency as the increment of concentration. In particular, 2, 3 and 4 showed highly effective protection properties. Specifically, the inhibition efficiencies for 2, 3 and 4 exceeded 95% when the concentration reached 40 mg L^{-1}, and finally got to approximately 98% at 200 mg L^{-1} with 3 as the best one. Thus the coupons in the presence of high concentrations of 2, 3 and 4 were well protected, with bright appearance highly similar to the new coupon (Fig. 4(a) and (b)). In addition, these four inhibitors contain various TPE cations and SCN$^-$ anions, thus they exhibit different solubility in aqueous. 1 and 2 are monovalent and divalent, respectively. So they were less soluble in aqueous and a mixed solvent of H_2O/ethanol was used to prepare each dense solution, which was added to 0.5 M H_2SO_4 reaching a final state of well-distributed suspension. 3 and 4 are trivalent and tetravalent, respectively, giving rise to higher solubility in aqueous. When

Fig. 4 Photographs of carbon steel coupons after weight-loss measurements under natural light, top view (a) and side view (b). Photograph of the coupons after weight-loss measurements under 365 nm UV light excitation (c). The sequences of the coupons in the photos are identical as follows, the coupons in the left side are blank sample and new coupon, respectively; from upper row to lower row are those respectively in the presence of 1, 2, 3 and 4 with concentration of 5, 10, 20, 40, 70, 100, and 200 mg L^{-1} from left to right.

they were added to the aggressive mediums, the solutions appeared almost homogeneous, especially for 4 even with its concentration as high as 200 mg L^{-1}.

In consideration of low concentration and high inhibiting efficiency, 2, 3 and 4 exert excellent inhibiting effect, compared with corrosion inhibitors for carbon steel in 0.5 M H_2SO_4 (Table S1†) or analogous acidic medium reported in literature.[3,8,10,23,45]

In contrast, the raw materials including NaSCN and amino-substituted tetraphenylethylene (**TPE-NH$_2$**, **TPE-2NH$_2$**, **TPE-3NH$_2$**, and **TPE-4NH$_2$**), exhibited negligible protecting effect for carbon steel, with inhibition efficiencies being less than 30% at any concentration (Fig. 5). Such huge contrast behaviors
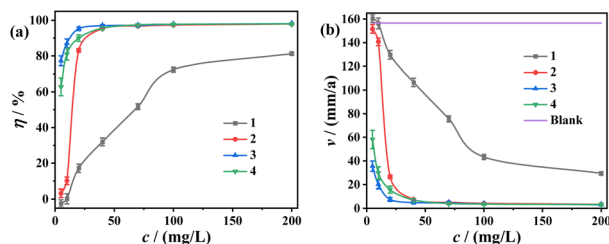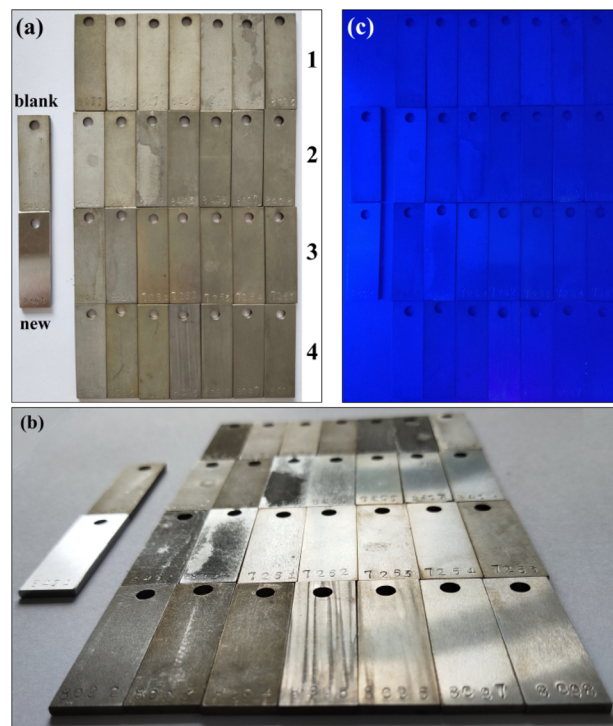

Fig. 3 Results of weight-loss measurements involving TPE-based inhibitors (1, 2, 3 and 4) for carbon steel coupons: (a) corrosion rate; (b) inhibition efficiency.
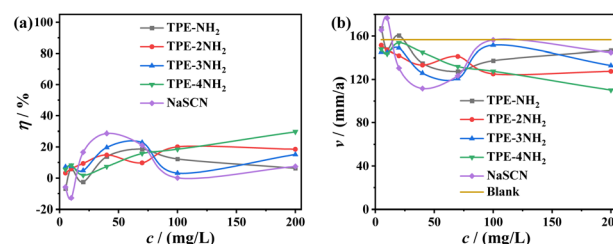

Fig. 5 Results of weight-loss measurements involving raw materials for carbon steel coupons: (a) corrosion rate; (b) inhibition efficiency.

between the TPE-based inhibitors and raw materials could be understood from two aspects: (1) hard and soft acids and bases (HSAB) theory;[46,47] (2) synergistic effect of the charged ingredients of the inhibitors.[5,48,49]

According to HSAB theory, Fe atom is classified as a soft Lewis acid with vacant electron orbitals, while thiocyanate anion (SCN⁻) is categorized as a soft Lewis base which is abundant with π electrons and lone pair electrons. Hence, SCN⁻ could form strong interaction with carbon steel surface, generating an electronegative surface. Due to the small spatial structure and low surface coverage on carbon steel surface, SCN⁻ alone could not effectively resist the aggressive attack of the highly corrosive medium. Therefore, NaSCN exhibited limited protection. While for the TPE-based inhibitors, after the adsorption of SCN⁻ and generation of an electronegative surface, the positive TPE cations would move forward to the surface driven by electrostatic attraction. Possessing larger hydrophobic skeletons, the TPE units would cover the surface more efficiently. And this would favor electron transfer from TPE units which is rich of π electrons to the metal surface. Hence, both the positive and negative ingredients of the TPE-based inhibitors would be adsorbed firmly to the surface, forming a protective film. Namely, there is adequate synergistic effect between the opposite charged ingredients. Nevertheless, as to amino-substituted tetraphenylethylene (**TPE-NH₂**, **TPE-2NH₂**, **TPE-3NH₂**, or **TPE-4NH₂**) alone, they could be easily protonated in the acidic medium, and hard to move toward the carbon steel surface which is also positively charged due to the corrosion and oxidation of Fe atoms.

As introduced above, TPE is a widely studied AIE agent. In aggregation state, the intramolecular motions will be restricted, including intramolecular rotations of the four peripheral phenyl rings around the central olefin, as well as molecular vibrations. In this study, the targeted TPE-based inhibitors (**1**, **2**, **3** and **4**) can protect carbon steel effectively in corrosive medium, as the form of adsorption film onto carbon steel surface.[22,45] Therefore, adsorption of the TPE-based inhibitors on metal surface would restrict the intramolecular rotations and molecular vibrations, thus should probably give rise to fluorescence emission under UV excitation, which has been reported on some other surfaces such as glass, polymer matrix, ice crystal and biointerfaces.[27,34,50] However, herein when the TPE-based inhibitors got adsorbed onto carbon steel surface, the coupons after weight-loss measurements were non-emissive under 365 nm UV light excitation, including those well protected coupons (Fig. 4(c)). In consideration of the intrinsic difference between metallic material and nonmetallic material, and fluorescence quenching of traditional fluorescent agents by heavy metal atoms,[35,51,52] it is understandable that the adsorption or aggregation of TPE-based inhibitors did not bring about fluorescence emission. To the best of our knowledge, aggregation of AIEgens always leads to fluorescence emission, while quenching of AIE fluorescence has not been reported up to date. The quenching process probably belongs to dynamic quenching, which takes place between the excited state of the inhibitors and Fe atoms. The excited state energy of the

inhibitors transfers to Fe atoms, and dissipates in a non-radiative relaxation manner, namely excited state energy transfer (EET).[53,54]

3.2 Adsorption isotherms

Basic information on the interaction between an organic inhibitor and metal surface could be obtained from various adsorption isotherms. Several typical types of adsorption isotherms are frequently used, such as Langmuir, Frumkin, Temkin, Freundlich, etc.[26,45] In this study, Langmuir adsorption isotherm was the better model for characterizing the inhibition process of these TPE-based inhibitors:

$$c/\theta = c + 1/K_{ads} \qquad (3)$$

where c represents the molar concentration of inhibitor; θ is the surface coverage for the coupon ($\theta = \eta$). K_{ads} denotes the adsorption–desorption equilibrium constant, obtained from the intercept of the c/θ *vs.* c plots (Fig. 6). Next, the standard Gibbs free energy of adsorption (ΔG_{ads}^0) can be acquired by K_{ads}, the universal gas constant (R) and thermodynamic temperature (T):

$$\Delta G_{ads}^0 = -RT\ln(55.5\,K_{ads}) \qquad (4)$$

In general, negative ΔG_{ads}^0 implies the adsorption process is thermodynamically spontaneous. When $\Delta G_{ads}^0 \geq -20$ kJ mol⁻¹, the electrostatic interaction between the inhibitor and metal surface is categorized as physisorption. While $\Delta G_{ads}^0 \leq -40$ kJ mol⁻¹, it is characterized as chemisorption, referring to the interaction involving charge sharing or transfer between the inhibitor molecules and metal surface. When ΔG_{ads}^0 lies between −20 kJ mol⁻¹ and −40 kJ mol⁻¹, it indicates a mix of physisorption and chemisorption.[3,16,23,45]

The calculated results are illustrated in Table 2. The high K_{ads} value and low ΔG_{ads}^0 value prove **2**, **3** and **4** can be spontaneously and firmly adsorbed on carbon steel surface, and the adsorptions belong to chemisorption. While for **1**, the adsorption is much more weaker, containing both physisorption and chemisorption.
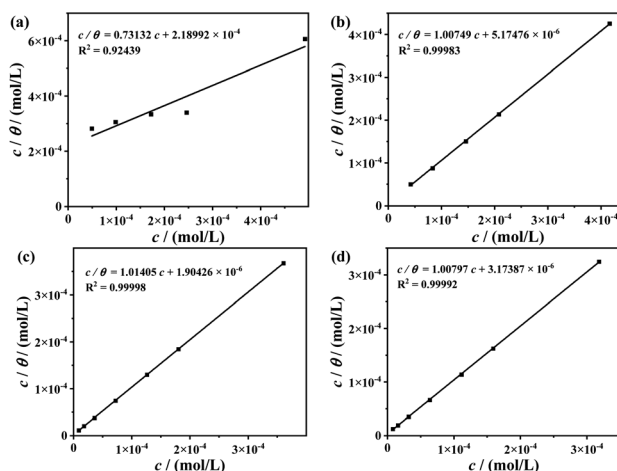

Fig. 6 Langmuir adsorption isotherms of (a) **1**, (b) **2**, (c) **3** and (d) **4** on carbon steel surface at 60 °C.

Table 2 Calculated results of the TPE-based inhibitors on carbon steel surface for Langmiur isotherm

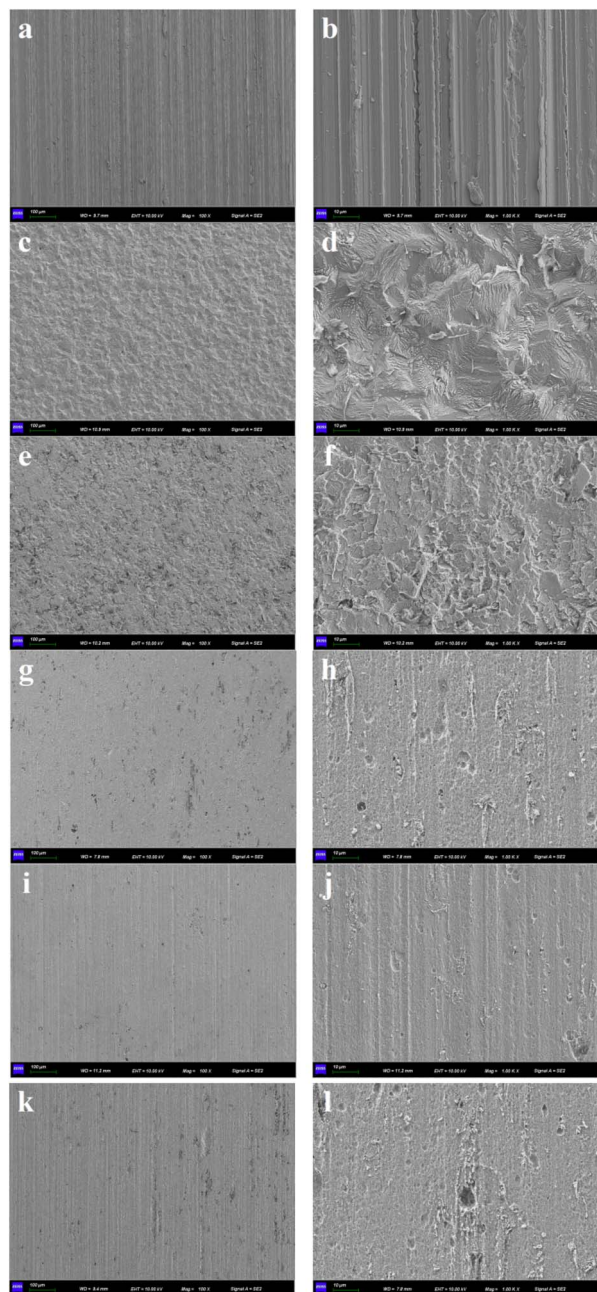| Inhibitor	Langmiur isotherm equation	$K_{ads}/(L\ mol^{-1})$	$\Delta G^0_{ads}/(kJ\ mol^{-1})$
1	$c/\theta = 0.73132\ c + 2.18992 \times 10^{-4}$	4.60233×10^3	-34.49
2	$c/\theta = 1.00749\ c + 5.17476 \times 10^{-6}$	1.93246×10^5	-44.84
3	$c/\theta = 1.01405\ c + 1.90426 \times 10^{-6}$	5.25138×10^5	-47.61
4	$c/\theta = 1.00797\ c + 3.17387 \times 10^{-6}$	3.15073×10^5	-46.20

Fig. 7 SEM images of carbon steel coupons: (a) and (b) new coupon; (c) and (d) blank sample after weight-loss measurement; in the presence of 200 mg L^{-1} **1** (e) and (f), **2** (g) and (h), **3** (i) and (j), **4** (k) and (l) after weight-loss measurements. Scale: 100 μm for (a, c, e, g, i and k) and 10 μm for (b, d, f, h, j and l).

3.3 Corrosion morphology

Surface morphological research on carbon steel coupons was carried out after weight-loss measurements. Fig. 7(a) and (b) display the scanning electron microscope (SEM) images of new coupon surface before corrosion, with clear and regular stripes. While the stripes were utterly demolished for the blank sample due to the severe corrosion by the aggressive medium, leaving a rough and bumpy surface (Fig. 7(c) and (d)). Nevertheless, for the samples in the presence of 200 mg L^{-1} TPE-based inhibitors, the destroy of coupon surface was greatly inhibited and the regular stripes were retained to a large extent, especially for **3** (Fig. 7(i) and (j)), then **4** (Fig. 7(k) and (l)) and **2** (Fig. 7(g) and (f)). The SEM images of the coupons in the presence of other concentrations of TPE-based inhibitors are provided in ESI (Fig. S1–S4†). With the increment of inhibitor concentration, the corrosion was gradually mitigated for each inhibitor.

3.4 Electrochemical study

Potentiodynamic polarization (PDP) curves were collected for carbon steel electrodes after 1 h immersion in both blank solution and the solutions with different concentrations of TPE-based inhibitors (Fig. 8(a) and S5†). The corresponding electrochemical data including corrosion current density (I_{corr}), corrosion potential (E_{corr}), cathodic (β_c) and anodic (β_a) Tafel slop, and corrosion inhibition efficiency (η_P), are listed in Table 3. The η_P was calculated by the following equation:

$$\eta_P = (1 - I_{corr}/I^0_{corr}) \times 100\% \tag{5}$$

where I^0_{corr} and I_{corr} are the corrosion current densities obtained in blank solution and solution with inhibitor, respectively. Generally, E_{corr} of carbon steel electrodes display positive shift after adding inhibitors, indicating that these TPE-based
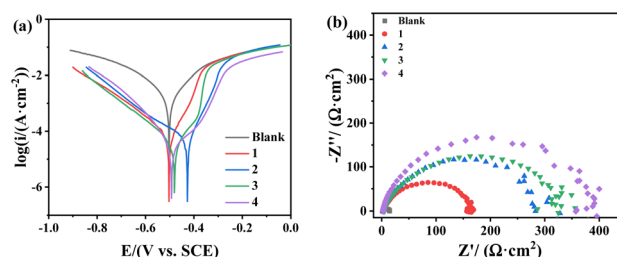

Fig. 8 (a) PDP curves and (b) EIS curves for carbon steel in the absence or presence of 100 mg L^{-1} TPE-based inhibitors.

Table 3 Electrochemical parameters of carbon steel in the absence or presence of 100 mg L^{-1} different TPE-based inhibitors by PDP and EIS measurements in 0.5 M H$_2$SO$_4$

Inhibitor	I_{corr}/(μA cm^{-2})	E_{corr}/V	β_c/(mV dec^{-1})	β_a/(mV dec^{-1})	η_P/%	R_s/(Ω cm^{-2})	R_{ct}/(Ω cm^{-2})	η_E/%
Blank	1701.0	−0.503	146.3	113.2	—	2.7	11.8	—
1	57.5	−0.502	141.7	48.1	96.6	2.8	162.3	92.7
2	55.1	−0.427	203.2	51.5	96.8	1.9	287.9	95.9
3	32.2	−0.481	140.7	44.5	98.1	3.8	331.5	96.4
4	35.6	−0.493	99.1	118.4	97.9	3.0	383.0	96.9

inhibitors tend to suppress corrosion process preferentially by affecting anodic reactions. Among the four inhibitors, **1** shows relatively weaker inhibition effect, especially when concentration is lower than 70 mg L^{-1} (Table S2†). In contrast, the calculated inhibition efficiencies of **2**, **3** and **4** exceed 90% even with dosage as low as 20 mg L^{-1}. When dosage reaching 100 mg L^{-1}, **2**, **3** and **4** effectively suppress corrosion current from 1701.0 μA cm^{-2} to 55.1, 32.2 and 35.6 μA cm^{-2}, and the inhibition efficiencies increase to 96.8%, 98.1% and 97.9%, respectively.

Electrochemical impedance spectroscopy (EIS) tests were carried out to provide supplementary inhibition evidence of the TPE-based inhibitors. Nyquist plots of carbon steel electrodes were collected at open-circuit potential (OCP) in 0.5 M H$_2$SO$_4$ and the solutions containing inhibitors (Fig. 8(b) and S6†). The as obtained EIS data are fitted to equivalent electric circuits as illustrated in Fig. 9, where R_s, R_f, R_{ct}, C_f, and C_{dl} represent solution resistance, film resistance, charge transfer resistance, film capacitance and double layer capacitance, respectively. The corresponding extracted impedance profiles are listed in Tables 3 and S3.† Specifically, R_s implies the resistance between reference electrode and working electrode, and the difference between impedance obtained at low frequency and high frequency indicate the R_{ct} of the system. The R_{ct} values exhibit dramatic increase from 11.8 Ω cm^{-2} to over hundred after addition of TPE-based inhibitors. Meanwhile, the loop increases along with inhibition concentration, which confirms the inhibition effect of these compounds by forming protective film on carbon steel surface (Fig. S6†). Inhibition efficiency (η_E) was calculated using R_{ct} based on the following equation:

$$\eta_E = (1 - R_{ct}^0/R_{ct}) \times 100\% \qquad (6)$$

where R_{ct}^0 and R_{ct} are charge transfer resistances in blank solution and solution with inhibitor. In contrast with the

rapid corrosion reaction occurred in blank solution, carbon steel in solution with TPE-based inhibitors undergo a much slower corrosion process. Relatively, **1** is more concentration-dependent that only exhibits high inhibition efficiency under high concentration, while inhibition efficiencies of **2**, **3** and **4** rapidly soar to over 90% with dosage as low as 20 mg L^{-1}. Nevertheless, these four inhibitors all display high
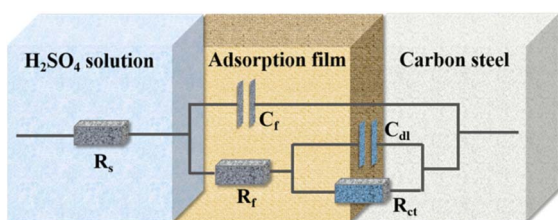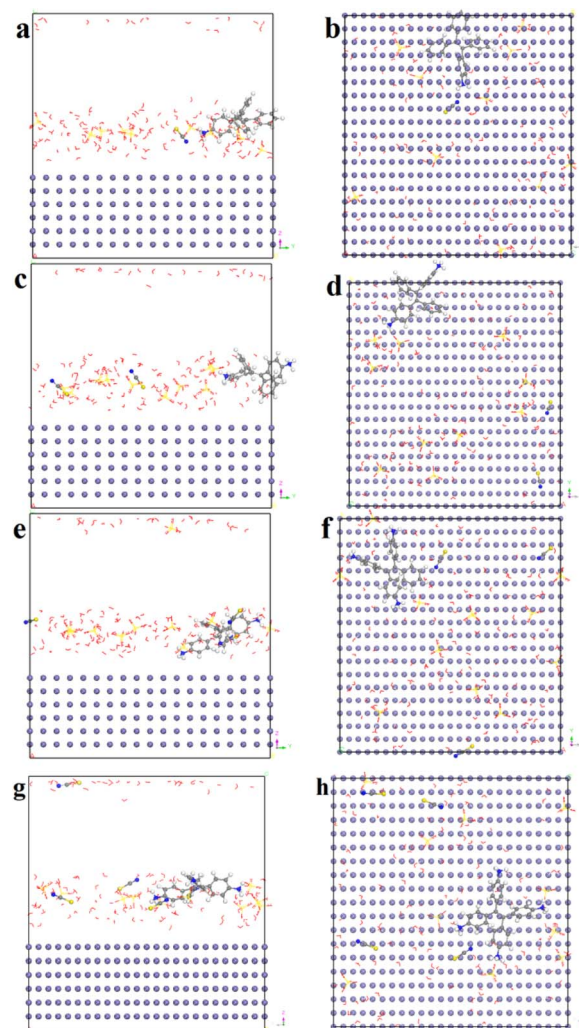

Fig. 10 Equilibrium adsorption configurations for the TPE-based inhibitors on carbon steel in solution. Side view (a) and top view (b) for **1**. Side view (c) and top view (d) for **2**. Side view (e) and top view (f) for **3**. Side view (g) and top view (h) for **4**. O atom: red; H atom: white; S atom: yellow; N atom: blue; C atom: gray.

Fig. 9 Proposed equivalent electrical circuit model used to fit EIS data for carbon steel in 0.5 M H$_2$SO$_4$ in presence of TPE-based inhibitors.

inhibition efficiencies of over 90% with concentration of 100 mg L^{-1}, reaching 92.7%, 95.9%, 96.4% and 96.9%, respectively. This is in consistent with the high inhibition efficiencies evidenced by weight-loss measurements and PDP analyses.

3.5 Theoretical calculations

In order to understand the adsorption behavior of the TPE-based inhibitors on carbon steel surface, Grand Canonical Monte Carlo (GCMC) was first carried out to investigate the stable adsorption configuration of the inhibitor molecules on a model surface in solution. The solution was presented with 1 neutral inhibitor molecule, $10H_2SO_4$ molecules and $100H_2O$ molecules. Fig. 10 illustrates the side and top views of the inhibitor molecules adsorbed on Fe (110) surface based on initial optimization and final adsorption, respectively. The results indicate that all the TPE-based inhibitors tend to move towards the Fe surface during the adsorption process, and eventually interact with the surface in forms of nearly flat stretched configuration. The inhibitor molecules and Fe atoms were displayed in ball and stick style, other molecules were displayed in line style.

In addition to the static adsorption configurations of four model inhibitors obtained from GCMC simulations, it is also necessary to investigate their anti-corrosion performance under actual flowing condition, a series of MD simulations were performed to model the dynamic adsorption capability of the TPE-based inhibitors on carbon steel surface. The model results of interaction energy (E_{int}) and binding energy ($E_{binding}$)[45] are illustrated in Table 4 and Fig. 11. The curve of SCN$^-$ is lower than that of SO$_4^{2-}$ which comes from the corrosive acid. And the curves of TPE cations (TPE$^+$, TPE^{2+}, TPE^{3+}, and TPE^{4+}) are lower than H$_3$O$^+$ as well. Hence, SCN$^-$ and TPE cations have more negative E_{int} or more positive $E_{binding}$ ($E_{binding} = -E_{int}$), indicating more intensive interactions of the ingredients of TPE-based inhibitors with carbon steel surface than the competing species from the corrosive medium. As for the neutral molecules, E_{int} follows the sequence **3** < **4** < **2** < **1** < H$_2$O, in agreement with the corrosion protection performance as discussed above.

Table 4 Interaction energy and binding energy values for species adsorbed on carbon steel surface

Species	E_{int}/(kJ mol^{-1})	$E_{binding}$/(kJ mol^{-1})
SCN$^-$	−2.179	2.179
SO$_4^{2-}$	−0.677	0.677
H$_3$O$^+$	−0.346	0.346
TPE$^+$	−8.316	8.316
TPE^{2+}	−9.662	9.662
TPE^{3+}	−6.970	6.970
TPE^{4+}	−7.885	7.885
H$_2$O	−0.501	0.501
1	−11.177	11.177
2	−16.813	16.813
3	−23.445	23.445
4	−22.243	22.243

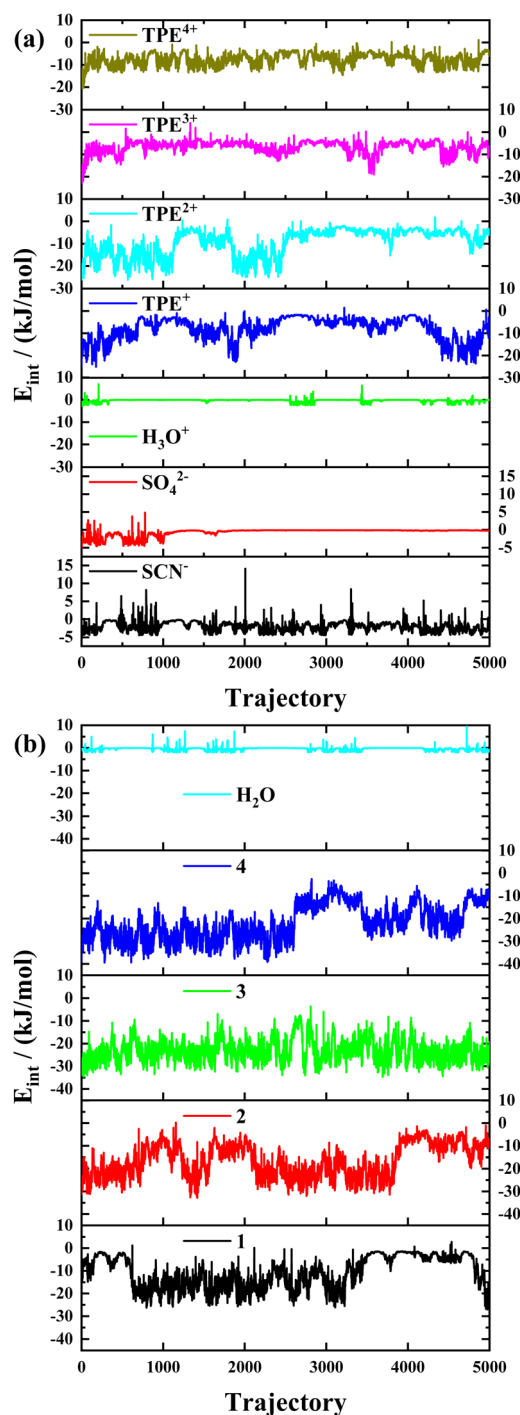**Fig. 11** E_{int} of (a) charged ions and (b) neutral molecules with carbon steel surface, respectively.

4. Conclusion

In summary, four novel corrosion inhibitors (**1**, **2**, **3** and **4**) in combination of TPE cations and SCN$^-$ were designed and synthesized. Weight-loss and electrochemical measurements manifested these inhibitors were effective corrosion inhibitors for carbon steel, particularly for **2**, **3** and **4** with inhibition efficiency exceeding 97%. In terms of HSAB theory and synergy

effect, both negatively charged SCN^- and positively charged TPE cations would get firmly adsorbed onto carbon steel surface, forming a protective film. GCMC and MD simulations were applied to explore the mechanism of the corrosion inhibition behaviors.

Author contributions

Yumeng Chen: methodology, investigation, formal analysis. Yiming An: formal analysis, investigation, writing – original draft. Jing Ma: formal analysis, investigation. Zhihua Zhang: methodology, investigation. Fulin Qiao: methodology, investigation. Xue Lei: investigation, formal analysis. Fei Sun: conceptualization, methodology, investigation, formal analysis, writing – review & editing, supervision, funding acquisition. Chunlu Wang: methodology, software, writing – review & editing. Song Gao: formal analysis, investigation. Yue Zhao: investigation, validation, writing – review & editing. Jinhua Wang: methodology, investigation. Xiaoping Fu: formal analysis. Hui Wang: formal analysis. Zhengqi Yu: methodology.

Conflicts of interest

The authors declare that they have no known competing financial interests or personal relationships that could have appeared to influence the work reported in this paper.

Acknowledgements

References

1 X. Li, D. Zhang, Z. Liu, Z. Li, C. Du and C. Dong, Materials science: Share corrosion data, *Nature*, 2015, **527**, 441–442.

2 B. Hou, X. Li, X. Ma, C. Du, D. Zhang, M. Zheng, W. Xu, D. Lu and F. Ma, The cost of corrosion in China, *npj Mater. Degrad.*, 2017, **1**, 4.

3 Y. Ye, D. Yang, H. Chen, S. Guo, Q. Yang, L. Chen, H. Zhao and L. Wang, A high-efficiency corrosion inhibitor of N-doped citric acid-based carbon dots for mild steel in hydrochloric acid environment, *J. Hazard. Mater.*, 2020, **381**, 121019.

4 A. V. Souza, J. C. da Rocha, J. A. C. Ponciano Gomes, L. C. M. Palermo and C. R. E. Mansur, Development and application of a passion fruit seed oil microemulsion as corrosion inhibitor of P110 carbon steel in CO_2-saturated brine, *Colloids Surf., A*, 2020, **599**, 124934.

5 H. Zhong, Z. Shi, G. Jiang and Z. Yuan, Synergistic inhibitory effects of free nitrous acid and imidazoline derivative on metal corrosion in a simulated water injection system, *Water Res.*, 2020, **184**, 116122.

6 J. Cui, Y. Yang, X. Li, W. Yuan and Y. Pei, Toward a Slow-Release Borate Inhibitor To Control Mild Steel Corrosion in Simulated Recirculating Water, *ACS Appl. Mater. Interfaces*, 2018, **10**, 4183–4197.

7 H. S. Gadow and M. Fakeeh, Green inhibitor of carbon steel corrosion in 1 M hydrochloric acid: Eruca sativa seed extract (experimental and theoretical studies), *RSC Adv.*, 2022, **12**, 8953–8986.

8 A. Rahimi, A. Farhadian, A. Berisha, A. Shaabani, M. A. Varfolomeev, V. Mehmeti, X. Zhong, S. Yousefzadeh and R. Djimasbe, Novel sucrose derivative as a thermally stable inhibitor for mild steel corrosion in 15% HCl medium: An experimental and computational study, *Chem. Eng. J.*, 2022, **446**, 136938.

9 E. D. Akpan, O. Dagdag and E. E. Ebenso, Recent progress on the anticorrosion activities of acridine and acridone derivatives: A review, *J. Mol. Liq.*, 2022, **361**, 119686.

10 L. Jiang, Y. Dong, Y. Yuan, X. Zhou, Y. Liu and X. Meng, Recent advances of metal-organic frameworks in corrosion protection: From synthesis to applications, *Chem. Eng. J.*, 2022, **430**, 132823.

11 H. Cen, C. Wu and Z. Chen, N, S, Co-doped carbon coated MnS/MnO/Mn nanoparticles as a novel corrosion inhibitor for carbon steel in CO_2-saturated NaCl solution, *Colloids Surf., A*, 2021, **630**, 127528.

12 C. Verma, S. H. Alrefaee, M. A. Quraishi, E. E. Ebenso and C. M. Hussain, Recent developments in sustainable corrosion inhibition using ionic liquids: A review, *J. Mol. Liq.*, 2021, **321**, 114484.

13 K. R. Ansari, D. S. Chauhan, M. A. Quraishi, A. Y. Adesina and T. A. Saleh, The synergistic influence of polyethyleneimine-grafted graphene oxide and iodide for the protection of steel in acidizing conditions, *RSC Adv.*, 2020, **10**, 17739–17751.

14 H. Cen, J. Cao and Z. Chen, Functionalized carbon nanotubes as a novel inhibitor to enhance the anticorrosion performance of carbon steel in CO_2-saturated NaCl solution, *Corros. Sci.*, 2020, **177**, 109011.

15 S. H. Alrefaee, K. Y. Rhee, C. Verma, M. A. Quraishi and E. E. Ebenso, Challenges and advantages of using plant extract as inhibitors in modern corrosion inhibition systems: Recent advancements, *J. Mol. Liq.*, 2021, **321**, 114666.

16 C. L. Wang and B. Qian, A novel l-histidine based ionic liquid (LHIL) as an efficient corrosion inhibitor for mild steel, *RSC Adv.*, 2022, **12**, 2947–2958.

17 B. Brycki and A. Szulc, Gemini surfactants as corrosion inhibitors. A review, *J. Mol. Liq.*, 2021, **344**, 117686.

18 F. Zhong, Y. He, P. Wang, C. Chen and Y. Wu, Novel pH-responsive self-healing anti-corrosion coating with high barrier and corrosion inhibitor loading based on reduced graphene oxide loaded zeolite imidazole framework, *Colloids Surf., A*, 2022, **642**, 128641.

19 M. Ouakki, M. Galai and M. Cherkaoui, Imidazole derivatives as efficient and potential class of corrosion inhibitors for metals and alloys in aqueous electrolytes: A review, *J. Mol. Liq.*, 2022, **345**, 117815.

20 C. Verma, M. H. Abdellattif, A. Alfantazi and M. A. Quraishi, N-heterocycle compounds as aqueous phase corrosion

inhibitors: A robust, effective and economic substitute, *J. Mol. Liq.*, 2021, **340**, 117211.

21 R. Aslam, G. Serdaroglu, S. Zehra, D. K. Verma, J. Aslam, L. Guo, C. Verma, E. E. Ebenso and M. A. Quraishi, Corrosion inhibition of steel using different families of organic compounds: Past and present progress, *J. Mol. Liq.*, 2022, **348**, 118373.

22 C. Verma and M. A. Quraishi, Recent progresses in Schiff bases as aqueous phase corrosion inhibitors: Design and applications, *Coord. Chem. Rev.*, 2021, **446**, 214105.

23 M. Cui and X. Li, Nitrogen and sulfur Co-doped carbon dots as ecofriendly and effective corrosion inhibitors for Q235 carbon steel in 1 M HCl solution, *RSC Adv.*, 2021, **11**, 21607–21621.

24 B. Lin, J. Wang, H. Zhang, Y. Wang, H. Zhang, J. Tang, J. Hou, H. Zhang and M. Sun, Self-healing performance of ethyl-cellulose based supramolecular gel coating highly loaded with different carbon chain length imidazoline inhibitors in NaCl corrosion medium, *Corros. Sci.*, 2022, **197**, 110084.

25 X. Zhao, C. Chen, Q. Sun, Y. Li and H. Yu, Molecular structure optimization design of inhibitors based on frontier orbitals theory, *Appl. Surf. Sci.*, 2019, **494**, 895–907.

26 M. M. Shaban, A. M. Eid, R. K. Farag, N. A. Negm, A. A. Fadda and M. A. Migahed, Novel trimeric cationic pyridinium surfactants as bi-functional corrosion inhibitors and antiscalants for API 5L X70 carbon steel against oilfield formation water, *J. Mol. Liq.*, 2020, **305**, 112817.

27 J. Mei, N. L. C. Leung, R. T. K. Kwok, J. W. Y. Lam and B. Z. Tang, Aggregation-Induced Emission: Together We Shine, United We Soar, *Chem. Rev.*, 2015, **115**, 11718–11940.

28 J. Luo, Z. Xie, J. W. Lam, L. Cheng, H. Chen, C. Qiu, H. S. Kwok, X. Zhan, Y. Liu, D. Zhu and B. Z. Tang, Aggregation-induced emission of 1-methyl-1,2,3,4,5-pentaphenylsilole, *Chem. Commun.*, 2001, 1740–1741.

29 Z. Zhu, Q. Wang, H. Liao, M. Liu, Z. Liu, Y. Zhang and W. Zhu, Trapping endoplasmic reticulum with amphiphilic AIE-active sensor via specific interaction of ATP-sensitive potassium (KATP), *Nat. Sci. Rev.*, 2021, **8**, nwaa198.

30 K. Siddharth, P. Alam, M. D. Hossain, N. Xie, G. S. Nambafu, F. Rehman, J. W. Y. Lam, G. Chen, J. Cheng, Z. Luo, G. Chen, B. Z. Tang and M. Shao, Hydrazine Detection during Ammonia Electro-oxidation Using an Aggregation-Induced Emission Dye, *J. Am. Chem. Soc.*, 2021, **143**, 2433–2440.

31 X. Wu, J. Wu, J. Dai, B. Chen, Z. Chen, S. Wang, F. Wu, X. Lou and F. Xia, Aggregation-induced emission luminogens reveal cell cycle-dependent telomerase activity in cancer cells, *Nat. Sci. Rev.*, 2021, **8**, nwaa306.

32 H. Ding, J. Li, G. Xie, G. Lin, R. Chen, Z. Peng, C. Yang, B. Wang, J. Sun and C. Wang, An AIEgen-based 3D covalent organic framework for white light-emitting diodes, *Nat. Commun.*, 2018, **9**, 5234–5240.

33 G. Huang, Q. Xia, W. Huang, J. Tian, Z. He, B. S. Li and B. Z. Tang, Multiple Anti-Counterfeiting Guarantees from a Simple Tetraphenylethylene Derivative - High-Contrasted and Multi-State Mechanochromism and Photochromism, *Angew. Chem., Int. Ed.*, 2019, **58**, 2–8.

34 Z. He, P. Liu, S. Zhang, J. Yan, M. Wang, Z. Cai, J. Wang and Y. Dong, A Freezing-Induced Turn-On Imaging Modality for Real-Time Monitoring of Cancer Cells in Cryosurgery, *Angew. Chem., Int. Ed.*, 2019, **58**, 3834–3837.

35 J. Mei, Y. Hong, J. W. Y. Lam, A. Qin, Y. Tang and B. Z. Tang, Aggregation-Induced Emission: The Whole Is More Brilliant than the Parts, *Adv. Mater.*, 2014, **26**, 5429–5479.

36 F. Sun, G. Zhang, D. Zhang, L. Xue and H. Jiang, Aqueous Fluorescence Turn-on Sensor for Zn^{2+} with a Tetraphenylethylene Compound, *Org. Lett.*, 2011, **13**, 6378–6381.

37 Z. Xie, P. Sun, Z. Wang, H. Li, L. Yu, D. Sun, M. Chen, Y. Bi, X. Xin and J. Hao, Metal-Organic Gels from Silver Nanoclusters with Aggregation-Induced Emission and Fluorescence-to-Phosphorescence Switching, *Angew. Chem., Int. Ed.*, 2019, **59**, 9922–9927.

38 F. Huo, Y. Liu, Y. Tang, Y. Cao, C. Tan, F. Yang and X. Yang, Aggregation induced emission of amino-thiol capped gold nanoparticles (GNPs) through metal-amino-coordination, *Colloids Surf., B*, 2019, **183**, 110335.

39 Z. Guo, G. Li, H. Wang, J. Zhao, Y. Liu, H. Tan, X. Li, P. J. Stang and X. Yan, Drum-like Metallacages with Size-Dependent Fluorescence: Exploring the Photophysics of Tetraphenylethylene under Locked Conformations, *J. Am. Chem. Soc.*, 2021, **143**, 9215–9221.

40 M. Li, S. Jiang, Z. Zhang, X.-Q. Hao, X. Jiang, H. Yu, P. Wang, B. Xu, M. Wang and W. Tian, Tetraphenylethylene-Based Emissive Supramolecular Metallacages Assembled by Terpyridine Ligands, *CCS Chem.*, 2021, **2**, 337–348.

41 A. H. Malik, A. Kalita and P. K. Iyer, Development of Well-Preserved, Substrate-Versatile Latent Fingerprints by Aggregation-Induced Enhanced Emission-Active Conjugated Polyelectrolyte, *ACS Appl. Mater. Interfaces*, 2017, **9**, 37501–37508.

42 T. L. M. Pham, T. K. Phung and H. V. Thang, DFT insights into the adsorption mechanism of five-membered aromatic heterocycles containing N, O, or S on Fe(110) surface, *Appl. Surf. Sci.*, 2022, **583**, 152524.

43 A. K. Rappe, C. J. Casewit, K. S. Colwell, W. A. Goddard and W. M. Skiff, UFF, a full periodic table force field for molecular mechanics and molecular dynamics simulations, *J. Am. Chem. Soc.*, 1992, **114**, 10024–10035.

44 P. Ma, Z. Zhang, W. Xu, Z. Teng, Y. Luo, C. Gong and Q. Wang, Integrated Portable Shrimp-Freshness Prediction Platform Based on Ice-Templated Metal-Organic Framework Colorimetric Combinatorics and Deep Convolutional Neural Networks, *ACS Sustainable Chem. Eng.*, 2021, **9**, 16926–16936.

45 T. K. Sarkar, M. Yadav and I. B. Obot, Mechanistic evaluation of adsorption and corrosion inhibition capabilities of novel indoline compounds for oil well/tubing steel in 15% HCl, *Chem. Eng. J.*, 2022, **431**, 133481.

46 F. H. Walters, Design of corrosion inhibitors: Use of the hard and soft acid-base (HSAB) theory, *J. Chem. Educ.*, 1991, **68**, 29–31.

47 X. Lei, Y. An, F. Qiao, Y. Chen, S. Gao, L. Zuo, Y. Zhao, F. Sun, C. Wang, B. Qin, Q. Zhuo, J. Wang, X. Fu, H. Wang and Z. Yu,

Fluorescence Turn-On Corrosion Inhibitor with a Tetraphenylethylene Framework: Corrosion Inhibition and Theoretical Calculations, *Adv. Mater. Interfaces*, 2022, **9**, 2201607.

48 Q. H. Zhang, Z. N. Jiang, Y. Y. Li, X. Wang, W. Xiong, H. F. Liu and G. A. Zhang, In-depth insight into the inhibition mechanism of the modified and combined amino acids corrosion inhibitors: "intramolecular synergism" vs. "intermolecular synergism", *Chem. Eng. J.*, 2022, **437**, 135439.

49 T. Zheng, J. Liu, M. Wang, Q. Liu, J. Wang, Y. Chong and G. Jia, Synergistic corrosion inhibition effects of quaternary ammonium salt cationic surfactants and thiourea on Q235 steel in sulfuric acid: Experimental and theoretical research, *Corros. Sci.*, 2022, **199**, 110199.

50 Y. Yang, G. B. Hu, W. B. Liang, L. Y. Yao, W. Huang, Y. J. Zhang, J. L. Zhang, J. M. Wang, R. Yuan and D. R. Xiao, An AIEgen-based 2D ultrathin metal-organic layer as an electrochemiluminescence platform for ultrasensitive biosensing of carcinoembryonic antigen, *Nanoscale*, 2020, **12**, 5932–5941.

51 P. C. Yeh, S. Yoon, D. Kurniawan, Y. G. Chung and W. H. Chiang, Unraveling the Fluorescence Quenching of Colloidal Graphene Quantum Dots for Selective Metal Ion Detection, *ACS Appl. Nano Mater.*, 2021, **4**, 5636–5642.

52 D. S. Rahman, S. Deb and S. K. Ghosh, Relativity of Electron and Energy Transfer Contributions in Nanoparticle-Induced Fluorescence Quenching, *J. Phys. Chem. C*, 2015, **119**, 27145–27155.

53 V. H. Pérez-Luna, S. Yang, E. M. Rabinovich, T. Buranda, L. A. Sklar, P. D. Hampton and G. P López, Fluorescence biosensing strategy based on energy transfer between fluorescently labeled receptors and a metallic surface, *Biosens. Bioelectron.*, 2002, **17**, 71–78.

54 Y. Zhang, T. S. Lee, J. M. Favale, D. C. Leary, J. L. Petersen, G. D. Scholes, F. N. Castellano and C. Milsmann, Delayed fluorescence from a zirconium(IV) photosensitizer with ligand-to-metal charge-transfer excited states, *Nat. Chem.*, 2020, **12**, 345–352.